

Analytical solution to simulate the behavior of reinforced concrete beams post-strengthened with FRP strips

Solução analítica para previsão do comportamento de vigas de concreto armado reforçadas com laminados de PRF

M. R. GARCEZ ^a

mrgarcez@hotmail.com

L. C. P. DA SILVA FILHO ^b

lcarlos66@gmail.com

Abstract

Aiming to develop an analytical solution to describe the behavior of reinforced concrete beams post-strengthened with FRP systems, with or without prestressing, a non-linear solution based on a tri-linear moment-curvature response was proposed. Three characteristic points were used to define the stages of the moment-curvature diagram: concrete cracking, steel yielding and ultimate capacity of the cross section. The load-deflection responses of the post-strengthened beams were then obtained by a double integration of the moment-curvature curve. This analytical procedure was implemented using the Matlab® software and the results obtained have closely matched the experimental data collected in bending tests performed in concrete beams post-strengthened with post-tensioned and non post-tensioned FRP strips.

Keywords: FRP, tri-linear analysis, analytical solution.

Resumo

Visando desenvolver uma solução analítica para prever o comportamento de vigas de concreto armado reforçadas com laminados de PRF, com ou sem protensão, uma solução não-linear foi proposta, assumindo um diagrama momento-curvatura com resposta tri-linear. Os pontos característicos adotados para definir os estágios do diagrama foram: a fissuração do concreto, o escoamento do aço e capacidade última do elemento reforçado. As deflexões foram obtidas pela dupla integração do diagrama momento-curvatura da seção transversal do elemento reforçado, sendo geradas as respostas carga-deslocamento. A solução analítica foi implementada usando o software Matlab® e os resultados gerados se mostraram compatíveis aos obtidos experimentalmente, em ensaios de flexão de vigas de concreto armado reforçadas com laminados de PRF protendidos e não-protendidos.

Palavras-chave: PRF, análise tri-linear, solução analítica.

^a Dra., Federal University of Pampa (UNIPAMPA), Researcher at LEME (Portuguese acronym of the Laboratory of Testing and Structural Modeling) of the Federal University of Rio Grande do Sul (UFRGS). E-mail: mrgarcez@hotmail.com

^b PhD., Federal University of Rio Grande do Sul (UFRGS), Researcher at LEME (Portuguese acronym of the Laboratory of Testing and Structural Modeling) of the Federal University of Rio Grande do Sul (UFRGS). E-mail: lcarlos66@gmail.com

1. Introduction

Since the 80's, when they began to be investigated and applied in Europe, Japan and the United States, Fiber Reinforced Polymers (FRP) have evolved to become one of the most popular techniques to post-strengthen reinforced concrete structures. In Brazil, the use of FRP has suffered a continuous increase, since the 90's, and many advances on research and field applications occurred in this time. One of the most promising involves the use of pre-stressing to make a better use of the very high tensile capacity of the composite.

Aiming to develop an analytical solution suitable to describe the behavior of reinforced concrete beams post-strengthened with both prestressed and non-prestressed FRP systems, a non-linear solution was proposed, based on state-of-the-art recommendations regarding the behavior of post-strengthened reinforced concrete elements. The analytical procedure did not require a high computational effort and was easily implemented using the MATLAB® software, a high-level technical computing language and interactive environment for algorithm development, data visualization, data analysis, and numeric computation.

2. Analytical model

The non-linear analytical model proposed was based on the concept that FRP behavior can be adequately represented by a tri-linear moment *versus* curvature relationship, as proposed by Charkas *et al.* [1], El-Mihilmy and Tedesco [3] and Razaqpur *et al.* [3]. The diagram used is therefore composed by three main stages, as shown in Figure [1]: pre-cracking stage or Stage I (from the initial application of the load up to the beginning of flexural cracking), post-cracking or Stage II (from initial cracking up to yielding of the steel reinforcement) and post-yielding or Stage III (from rebar yield until concrete or FRP failure). Load *versus* deflection at mid-span diagrams were then obtained by double integration of the moment *versus* curvature diagrams.

At Stage I, the bending moment (M) on the cross-section is lower than the cracking moment, M_{cr} . At Stage II, the bending moment surpass M_{cr} but is lower than the moment that produces the yielding of the steel rebar, M_y . At Stage III, the bending moment on the cross-section is higher than M_y and lower than M_u , representing the ultimate moment of the cross-section.

Moments and curvatures were calculated based on the strain compatibility and equilibrium condition of forces for the rectangular cross section of a reinforced concrete beam post-strengthened with non-prestressed FRP strips.

Figure 1- Tri-linear moment *versus* curvature response of FRP post-strengthened reinforced concrete sections

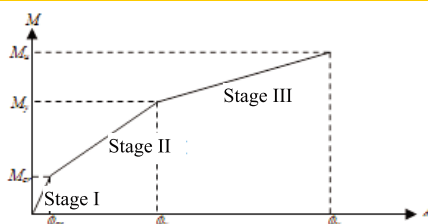


Figure 2 – Stress-strain diagram for rectangular sections of FRP post-strengthened reinforced concrete beams

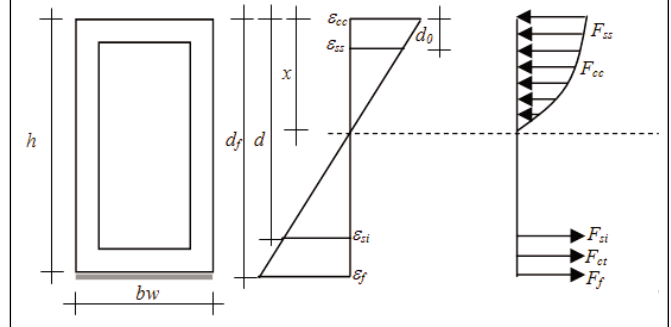


Figure [2] shows the stress-strain diagram for rectangular sections of non-prestressed FRP post-strengthened reinforced concrete beams, used to verify the internal equilibrium of forces in each stage.

The equilibrium of the internal sectional forces is given by Equation [1], as follow:

$$F_{cc} + F_{ss} = F_{si} + F_{ct} + F_f \quad (1)$$

Where:

F_{cc} – Resulting compressive force in concrete.

F_{ss} – Resulting compressive force in steel reinforcement at upper edge of cross-section.

F_{si} – Resulting tensile force in steel reinforcement at lower edge of cross-section.

F_{ct} – Resulting tensile force in concrete.

F_f – Resulting tensile force in FRP.

Concrete in compression was assumed to behave linearly up to an extreme fiber stress of 70% of its compressive strength (Eq. [2]), after which the parabolic curve proposed by Hognestad, described in Charkas *et al.* (2003), was used (Eq. [3]).

$$\sigma_{ct} = E_c \varepsilon_{ct} \quad (2)$$

$$\sigma_{cc} = f_c \left[2 \frac{\varepsilon_{cc}}{\varepsilon_{cu}} - \left(\frac{\varepsilon_{cc}}{\varepsilon_{cu}} \right)^2 \right] \quad (3)$$

Where:

E_c – Young's modulus of concrete.

f_c – Compressive strength of concrete.

ε_{cc} and ε_{ct} – Compressive strain of concrete at upper edge of cross-

section and tensile strain of concrete at lower edge of cross-section.
 ϵ_{cu} – Strain corresponding to compressive strength of concrete.
 σ_{cc} and σ_{ct} – Compressive stress of concrete at upper edge of cross-section and tensile stress of concrete at lower edge of cross-section.

Steel was considered as a perfectly elastoplastic material, defined by its yielding stress. Eq. [4] and Eq. [5] represent the behavior of steel before and after yielding.

$$\sigma_s = E_s \epsilon_s \quad (4)$$

$$\sigma_s = f_y \quad (5)$$

Where:

E_s – Young’s modulus of steel.

f_y – Yielding stress of steel.

ϵ_s – Strain of steel.

σ_s – Stress of steel.

The post-strengthening material (FRP strips) was assumed to behave linearly up to failure (Eq. [6]):

$$\sigma_f = E_f \epsilon_f \quad (6)$$

Where:

E_f - Young’s (or elasticity) modulus of FRP.

ϵ_f – Strain of FRP.

Once the constitutive stress-strain laws for each material were defined, the equilibrium of the internal forces - for each one of the three stages described previously - could be rewritten as follows. Considering Stage 1, the Equation [1] was rewritten as Equation [7]:

$$bw \int_0^x \sigma(y) dy + \epsilon_{ss} E_s A_{ss} = \epsilon_{si} E_s A_{si} + \epsilon_{ct} E_c A_{ct} + \epsilon_f E_f A_f \quad (7)$$

Where:

$\sigma(y)$ – Function that represents the behavior of concrete under compression.

The strain compatibility equations for a post-strengthened reinforced concrete cross-section were used in Equation [7] to obtain Equation [8].

$$bw f_c \frac{\epsilon_{cc}}{\epsilon_{cu}} \left(1 - \frac{\epsilon_{cc}}{3\epsilon_{cu}}\right) x + \epsilon_{cc} \left(\frac{x-d_0}{x}\right) E_s A_{ss} = \epsilon_{cc} \left(\frac{d-x}{x}\right) E_s A_{si} + \epsilon_{cc} \left(\frac{h-x}{x}\right) E_c bw \left(\frac{h-x}{2}\right) + \epsilon_{cc} \left(\frac{d_f-x}{x}\right) E_f A_f \quad (8)$$

Equation [9] shows the second order polynomial that expresses

the equilibrium at Stage I.

$$\left(\frac{2p}{\epsilon_{cc}} - E_c bw\right) x^2 + (2E_s A_{ss} + 2E_c bw h + 2E_s A_{si} + 2E_f A_f) x - (2d_0 E_s A_{ss} + bw E_c h^2 + 2d E_s A_{si} + 2d_f E_f A_f) = 0 \quad (9)$$

Where:

$$p = bw f_c \frac{\epsilon_{cc}}{\epsilon_{cu}} \left(1 - \frac{\epsilon_{cc}}{3\epsilon_{cu}}\right) \quad (10)$$

A_{ss} – Area of steel reinforcement at upper edge of cross-section.

A_{si} – Area of steel reinforcement at lower edge of cross-section.

A_f – Area of FRP strips.

After Stage I, concrete reached its tensile strength, and Equation [1] may be rewritten as Equation [11], that represents Stage II:

$$bw \int_0^x \sigma(y) dy + \epsilon_{ss} E_s A_{ss} = \epsilon_{si} E_s A_{si} + \epsilon_f E_f A_f \quad (11)$$

Strain compatibility equations were then applied on equation [11] to obtain Equation [12].

$$bw f_c \frac{\epsilon_{cc}}{\epsilon_{cu}} \left(1 - \frac{\epsilon_{cc}}{3\epsilon_{cu}}\right) x + \epsilon_{cc} \left(\frac{x-d_0}{x}\right) E_s A_{ss} = \epsilon_{cc} \left(\frac{d-x}{x}\right) E_s A_{si} + \epsilon_{cc} \left(\frac{d_f-x}{x}\right) E_f A_f \quad (12)$$

Equation [13] shows the second order polynomial that expresses the equilibrium at Stage II.

$$px^2 + (\epsilon_{cc} E_s A_{ss} + \epsilon_{cc} E_s A_{si} + \epsilon_{cc} E_f A_f) x - (\epsilon_{cc} d_0 E_s A_{ss} + \epsilon_{cc} d E_s A_{si} + \epsilon_{cc} d_f E_f A_f) = 0 \quad (13)$$

At the end of Stage II, it can be assumed that the reinforcement steel placed at the lower edge of cross-section has already reached its yielding stress. Therefore, Equation [1] may be rewritten as:

$$bw \int_0^x \sigma(y) dy + \epsilon_{ss} E_s A_{ss} = f_y A_{si} + \epsilon_f E_f A_f \quad (14)$$

Equation [15] may then be obtained using strain compatibility equations in equation [13].

$$bw f_c \frac{\epsilon_{cc}}{\epsilon_{cu}} \left(1 - \frac{\epsilon_{cc}}{3\epsilon_{cu}}\right) x + \epsilon_{cc} \left(\frac{x-d_0}{x}\right) E_s A_{ss} = f_y A_{si} + \epsilon_{cc} \left(\frac{d_f-x}{x}\right) E_f A_f \quad (15)$$

Equation [16] shows the second order polynomial expression that represents the equilibrium condition at Stage III.

$$px^2 + (\epsilon_{cc} E_s A_{ss} + f_y A_{si} + \epsilon_{cc} E_f A_f) x - (\epsilon_{cc} d_0 E_s A_{ss} + \epsilon_{cc} d_f E_f A_f) = 0 \quad (16)$$

Neutral axis depth of the cross section for each one of the three stages as well as stresses and strains in concrete, steel reinforcement and FRP strips are calculated through iterative processes, involving equations [9], [13] and [16]. Each stage is fully defined once its stresses and strains are determined: this means, at Stage I, the stress and strain that causes concrete to crack; at Stage II, the stress and strain that causes the yielding of the steel reinforcement; and, at Stage III, the stress and strain that causes concrete crushing or post-strengthening rupture.

After each stage is fully defined, as described on the last paragraph, bending moments and curvatures for Stages I, II and III are calculated. According to El-Mihilmy & Tedesco [3], Equation [17] describes the cracking moment M_{cr} , the maximum moment calculated at Stage I.

$$M_{cr} = \frac{f_t' I_g}{y} \quad (17)$$

Where:

f_t' – Modulus of rupture of concrete.

I_g – Moment of inertia of the gross concrete section.

y – Distance from the neutral axis of the gross concrete section to the extreme fiber.

Equation [18] may be used to calculate the curvature at this point, ϕ_{cr} .

$$\phi_{cr} = \frac{M_{cr}}{E_c I_g} \quad (18)$$

El-Mihilmy and Tedesco [3] suggest the use of Equation [19] to calculate the maximum moment of Stage II, M_y .

$$M_y = E_c I_{cr} \phi_y \quad (19)$$

Where:

I_{cr} – Moment of inertia of cracked section transformed to concrete (Stage II).

ϕ_y – Curvature that corresponds to yielding of steel.

Equation [20] may be used to calculate the curvature that corresponds to yielding of steel.

$$\phi_y = \frac{\epsilon_y}{d-x} \quad (20)$$

The ultimate moment (M_u) and curvature (ϕ_u) will be determined, according to Charkas *et al.* [2], based on the mode of failure: crushing of concrete or FRP rupture. If the failure mode is FRP rupture, Equation [21] may be used to calculate M_u . In case of concrete crushing before FRP rupture, Equation [22] may be used to calculate M_u .

$$M_u = A_{si} f_y (d - \gamma c) + A_f f_{fu} (d_f - \gamma c) + A_{ss} \sigma_{ss} (\gamma c - d_0) \quad (21)$$

$$M_u = A_{si} f_y \left(d - \frac{\beta_1 x}{2} \right) + A_f \sigma_f \left(d_f - \frac{\beta_1 x}{2} \right) + A_{ss} \sigma_{ss} (\gamma x - d_0) \quad (22)$$

Where:

$$\gamma = \frac{4\epsilon_{cu} - \epsilon_{cc}}{4(3\epsilon_{cu} - \epsilon_{cc})} \quad (23)$$

f_{fu} – Ultimate tensile strength of FRP.

β_1 – Relationship between depth of rectangular gross concrete section and neutral axis depth.

σ_{ss} – Stress of steel reinforcement at upper edge of cross-section. According to Razagpur *et al.* [3], Equations [24] and [25] may be used to calculate the curvature (ϕ_u), that corresponds to M_u , at the limit of Stage III, depending on the mode of failure. If ultimate failure occurs due to FRP rupture, ϕ_u is calculated through Equation [24]:

$$\phi_u = \frac{\epsilon_f}{d_f - x} \quad (24)$$

In case of concrete crushing before FRP rupture, ϕ_u is calculated through Equation [25]:

$$\phi_u = \frac{\epsilon_{cu}}{x} \quad (25)$$

The anchorage strength model developed by Teng *et al.* [6], based on the effective bond length of FRP, was used to determine the ultimate bond strength of FRP. In this approach, the ultimate bond strength is linear up to β_p , taking the form shown in Equation [26], which considers the width of the concrete member (bw) and the width of the FRP strip (L_f).

$$\beta_p = \sqrt{\left(2 - \frac{L_f}{bw} \right) \left(1 + \frac{L_f}{bw} \right)} \quad (26)$$

Equation [27] may be used to calculate the effective bond length (L_e) of FRP.

$$L_e = 0,5623 \sqrt{\frac{t_f E_f}{\sqrt{f_c}}} \quad (27)$$

Where:

t_f – Thickness of PRF.

The ultimate bond strength of FRP (F_{fu}) is given by Equation [28].

$$F_{fu} = 0,3162 \beta_p \beta_l \sqrt{f_c} L_f L_e \quad (28)$$

β_l expresses the relationship between bond length, L , and effective bond length, L_e , as shown by Equations [29] and [30].

$$\beta_l = 1, \text{ se } L \geq L_e \quad (29)$$

$$\beta_l = \text{sen} \left[\frac{\pi L}{2L_e} \right] \quad (30)$$

Equation [31] may be used to calculate the bond length L .

$$L = \frac{f_{fu} t_f}{\tau_{bu}} \quad (31)$$

Where:

τ_{bu} - Ultimate bonding strength, in MPa.

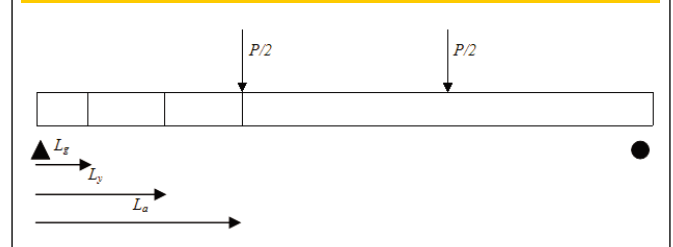
According Teng *et al.* [6], stress in the FRP strip at failure (kN/cm^2) is given by Equation [32]:

$$f_{fu} = 0,1956 \beta_p \beta_l \sqrt{\frac{E_f \sqrt{f_c}}{t_f}} \quad (32)$$

Once moments and curvatures corresponding to Stages I, II e III are defined, the procedure to determine vertical displacements is initiated.

Figure [1] shows that flexural rigidity of post-strengthened beams is reduced with the increase of moments. Considering that flexural rigidity is modified during loading, Charkas *et al.* [1] developed a procedure in which the effective flexural rigidity of the section varies along the beam depending on its moment diagram. This means considering how cracking affects the flexural rigidity along different sections of the beam. The stiffness distribution is accounted for by dividing the beam into three regions, namely uncracked (L_u), par-

Figure 3 – Flexural stiffness distribution in four-point bending



tially cracked (L_y) and subjected to post-yielding. Figure [3] shows the stiffness distribution for a simply supported post-strengthened reinforced concrete beam subjected to four-point bending, where L_a is the shear span.

Considering a simple supported beam, subjected to four-point bending, the integration provides the following expression to calculate the deflection at mid-span:

$$\delta_{\text{máx}} = \frac{\phi_a (3L^2 - 4L_a^2)}{24} + \frac{L_y}{6} [\phi_{cr} (L_y + L_g) - \phi_a (L_y + L_a)] + \frac{\phi_y (L_a - L_g)(L_a + L_y + L_g)}{6} \quad (33)$$

Where:

ϕ_a – Curvature corresponding to a given applied moment.

L_a – Shear span.

L_g e L_y are calculated using Equations [34] and [35]:

$$L_g = \frac{2M_{cr}}{P} \quad (34)$$

$$L_y = \frac{2M_y}{P} \quad (35)$$

Where:

P = Load applied on the beam.

Equation [33] is simplified for beams at Stage II, by substituting $L_y = L_a$, and, at Stage I, by substituting $L_g = L_a$, resulting in Equations [36] e [37].

$$\delta_{\text{máx}} = \frac{\phi_a (3L^2 - 4L_a^2)}{24} + \frac{(L_g + L_a)}{6} (\phi_{cr} L_a - \phi_a L_g) \quad (36)$$

$$\delta_{\text{máx}} = \frac{\phi_a (3L^2 - 4L_a^2)}{24} \quad (37)$$

Figure 4 – Stress-strain diagram for rectangular sections of prestressed FRP post-strengthened reinforced concrete beams: (a) Cross-section; (b) Initial strains due to prestressing; (c) Strains during loading; (d) Resultant internal forces

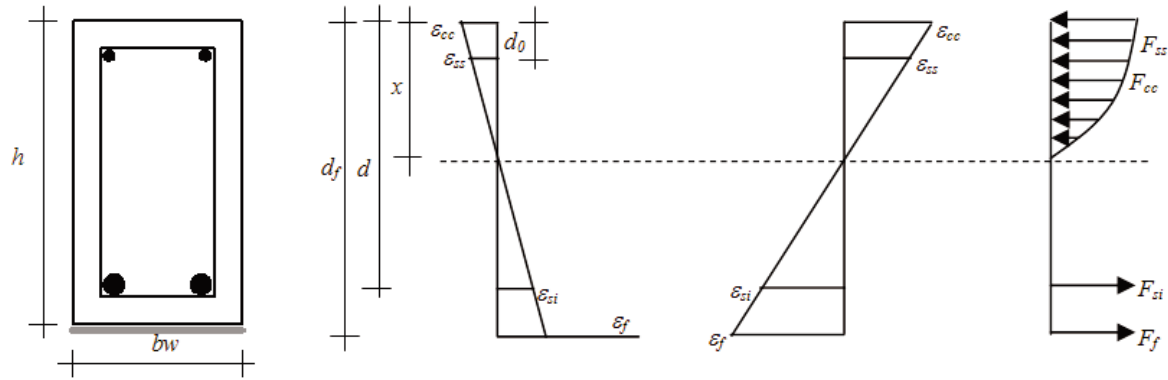


Figure [4] shows the stress-strain diagram for rectangular sections of prestressed FRP post-strengthened reinforced concrete beams. As seen in Figure [4](a), the strains and stresses due to the application of prestressing are planned to oppose the ones originated by the applied loads. Equations [38] and [39] may be used to calculate the normal tension in the top and bottom fibers of the cross-section in this situation.

$$\sigma_{cc} = \frac{-N_p}{Ac} + \frac{e_p}{W_{ss}} \quad (38)$$

$$\sigma_{ct} = \frac{-N_p}{Ac} - \frac{e_p}{W_{si}} \quad (39)$$

Where:

e_p – Eccentricity of prestressing force.

N_p – Final prestressing force.

W_{ss} e W_{si} – Section modulus with respect to upper and lower edges of cross-section.

It is important to consider that, as other prestressed structures, reinforced concrete beams post-strengthened with prestressed FRP are subjected to losses in the confining stress due to instantaneous or time-dependent effects. Losses due to elastic shortening of concrete are instantaneous. Losses due to creep, shrinkage and relaxation of FRP are time-dependent. Such losses must be deducted from the initial prestressing force.

Strains at upper and lower edges of the concrete cross-section may be defined, since stresses on the concrete due to prestressing application (σ_{ct} e σ_{cc}) are known.

Equation [40] shows how to determine the moment M_0 generated by an opposite stress on the concrete at the bottom face of the cross-section ($-\sigma_{ct}$), with the same value of the stress on the con-

crete at the lower edge of the concrete cross-section, determined by Equation [39].

$$M_0 = \frac{-\sigma_{ct} I}{y} \quad (40)$$

Once moment M_0 is applied on the cross-section, stresses (σ_{cc} e σ_{ct}) may be re-calculated and strains on the concrete cross-section may be determined, through Equations [41] and [42]. Such strains, determined by Equations [41] and [42], represent an initial state, prior to loading, originated by the applied prestressing force.

$$\epsilon_{cc} = \frac{\sigma_{cc}}{E_c} \quad (41)$$

$$\epsilon_{ct} = \frac{\sigma_{ct}}{E_c} \quad (42)$$

$$\phi_0 = \frac{-\epsilon_{cc} + \epsilon_{ct}}{h} \quad (43)$$

Where:

ϕ_0 – Initial curvature due to prestressing.

After determining the initial state, originated by the prestressing force applied on the cross section, the neutral axis depths of the cross section, as well as stresses and strains in concrete, steel reinforcement and FRP strips are calculated by means of an itera-

Table 1 - Experimental program

Beams	Post-Strengthening	Prestressing level
VT	No post-strengthened	-
VFC_NP_01	Two CFRP non-prestressed strips	-
VFC_PE_01	Two CFRP prestressed strips	35% of ϵ_{fu}

tive process, as described previously, for non-prestressed strips. However, the initial moment M_0 and the initial curvature ϕ_0 , must be added to the values of the moments and curvatures determined in each stage.

When prestressed strips are used, the ultimate strength of the FRP may be reached, depending, mainly, on the anchorage system and the post-strengthening configuration. However, if the anchorage system is not efficient, post-strengthening fails prematurely, before the ultimate strength of the FRP is reached.

3. Experimental procedure used to validate the analytical results

Results of the experimental program developed by Garcez [7] were used to validate the proposed analytical solution. The experimental program was based on bending tests performed on reinforced concrete beams post-strengthened, in the laboratory, with prestressed and non-prestressed Carbon Fiber Reinforced Polymers (CFRP) strips. A short description of the experimental specimens is given in Table [1].

The reinforced concrete beams tested were 6600mm long and had a rectangular cross-section 1000mm wide by 220mm deep. All beams were reinforced with seven bottom 12mm steel rebar (CA-50 steel), resulting in a reinforcement ratio $\rho = 0.0041$. The shear reinforcement consisted of 8mm steel stirrups spaced each 90mm, corresponding to $11.17\text{cm}^2/\text{m}$. Beams were post-strengthened with two strips (50x1.2mm) of CFRP. The prestressing level applied on the strips of the beam named VFC_PE_01 was 35% of ϵ_{fu} .

The concrete used to make the beams was produced at EMPA, in Switzerland, where the bending tests were conducted. The average 28-day cubic compressive strength, measured according to the EN 206-1 recommendations, was 44MPa.

In order to collect the necessary data for the numerical analysis, samples of the steel rebar used were submitted to tensile tests, according to EN 10002-1. The 8mm rebar had average values of 554MPa for yield stress, 2.51‰ for yield strain, 662MPa for ultimate stress and 220GPa for Young's modulus. The average values for the 12mm steel rebars were 436MPa, 1.98‰, 688MPa e 215GPa, respectively.

Table 2 - Post-strengthening system characteristics, provided by manufacturers

	Carbodur S 512 Strip	
Thickness (mm)	1,2	
Width (mm)	50	
Tensile Strength (MPa)	2.800	
Ultimate Strain (o/oo)	17	
Young's Modulus (MPa)	165,000	
	Sikadur®-30 Resin	Sikadur®-30LP Resin
Components	3Part A:1Part B	2Part A:1Part B
Pot life at 25°C (min)	-	60
Pot life at 35°C (min)	40	-
Pot life at 55°C (min)	-	30
Tg (°C)	62	107
Young's Modulus (MPa)	12.800	10,000

Figure 5 - Six-point bending test scheme

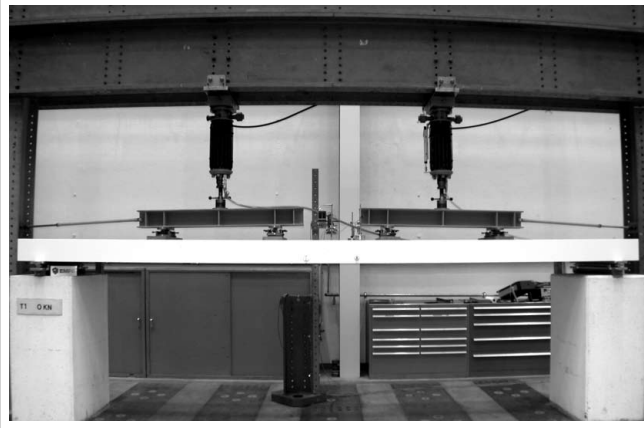


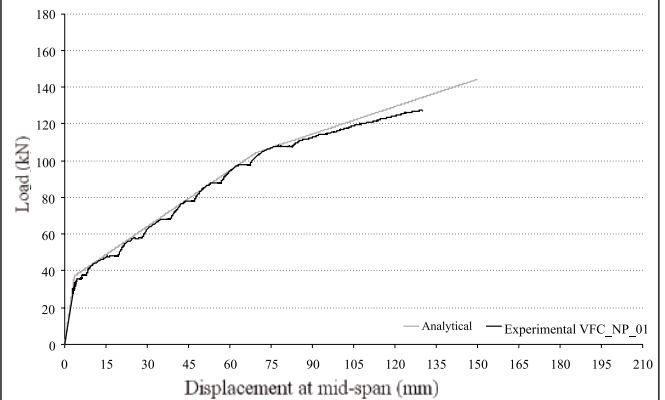
Table [2] shows some characteristics of the Sika® Carbodur post-strengthening system used in the tests. This system is composed of a carbon fiber strip, named Carbodur S 512, and an adhesive formulation, named Sikadur®-30. The adhesive Sikadur®-30LP, which has a longer pot life than normal formulations, was used to bond the prestressed strips to concrete.

The reinforced beams were subjected to six-point bending tests. In these tests the beams were simply supported and received four vertical loads, spaced 1200mm, as shown in Figure [5]. More information about the experimental procedures can be found at Garcez [7]. During the tests, deflections at mid-span and specific strains at steel, concrete and CFRP were continuously recorded by a computer controlled data acquisition system.

4. Analytical versus experimental results

A comparison between the experimental data and the results obtained through the proposed analytical procedure described in this

Figure 7 - Load versus vertical displacement at mid-span for beam VFC_NP_01



paper is shown in Table [3]. In the table it is possible to check the load values (P_{exp} and P_{num}) and vertical displacements at mid-span (δ_{exp} and δ_{num}), obtained in both cases, for the three stages of the load versus displacement diagrams.

Curves showing a plot of the analytical and experimental loads versus the displacement at mid-span for the control (VT) and post-strengthened (VFC_NP_01 and VFC_PE_01) beams can be seen in Figures 6 to 8. Meanwhile, Figures [9] and [10] show two failure modes observed on the post-strengthened beams: a peeling-off that occurred on beam VFC_NP_01 and the rupture of a CFRP strip on beam VFC_PE_02.

The examination of the data showed in Table [3] indicates that the proposed analytical solution adequately reproduces the behavior of the post-strengthened beams. In general, the differences between estimated and real loads at cracking, yielding and failure were lower than 5%. Differences of around 16.2% and 11% were registered on the estimated vertical displacement at mid-span near failure for beams VFC_NP_01 e VFC_PE_01, post-strengthened

Figure 6 - Load versus vertical displacement at mid-span for beam VT

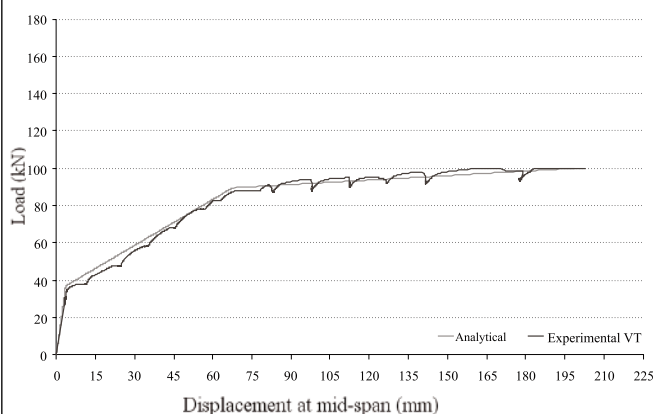


Figure 8 - Load versus vertical displacement at for beam VFC_PE_01

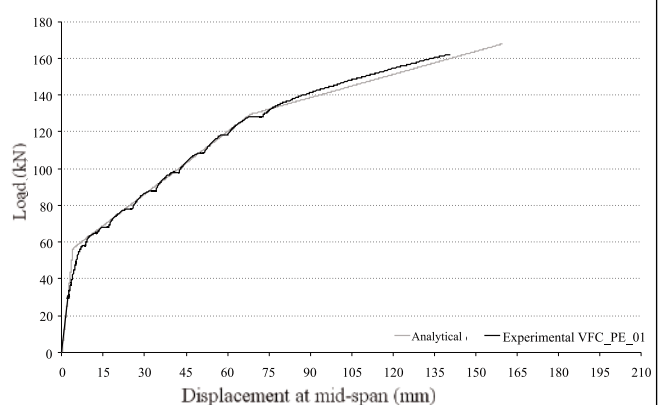
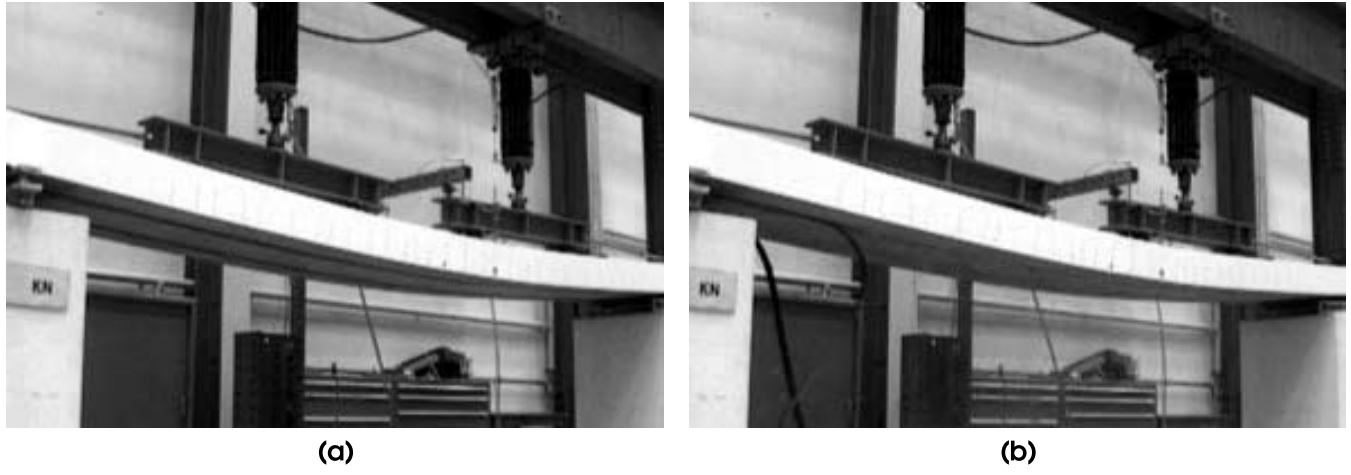


Figura 9 – Beam VFC_NP_01: (a) During testing; (b) After premature rupture of CFRP strips



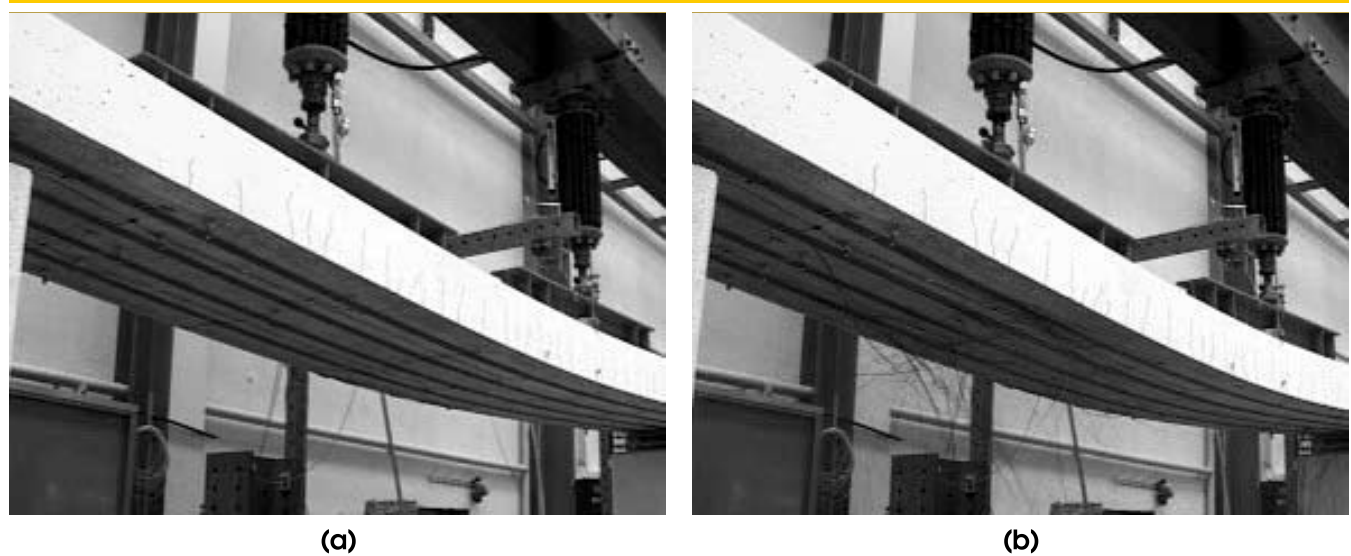
with two non-prestressed CFRP strips and two prestressed CFRP strips, respectively. The difference of 47.6% on the displacement at mid-span, noted on the first phase of the diagram of beam VFC_PE_01, was the most significant, considering all range of data.

Figure [6] provides evidence that the analytical solution was also a good representation of the behavior of the control beam (VT). The cracking load obtained through the analytical solution was practically the same registered experimentally. The displacement at mid-span, corresponding to the cracking load, was 2.6% higher than the one obtained experimentally. At yielding, the theoretical load and displacement values at mid-span were, respectively, 1.7% higher and 5.4% lower than the ones obtained experimentally. The failure mode of the control beam was the same for the experi-

ment and the analytical solution: crushing of concrete after yielding of steel. On the analytical procedure, the third phase of the load versus displacement diagram represents the use of the compressive strength of concrete, after yielding. In this case, as pointed out in Table [3], the simulation ended at the moment that the ultimate load, obtained from the experiment of beam VT, was reached.

Figure [7] and Table [8] present experimental and analytical results for beam VFC_NP_01. It can be observed in the figure that the experimental and analytical curves start to diverge at the third phase of the diagram, due to a premature failure of the CFRP, not considered in the analytical model. This is probably why the ultimate failure load, obtained from the analytical procedure, was 10.7% higher than the load obtained experimentally for this beam.

**Figure 10 – Beam VFC_PE_02: (a) During testing;
(b) After ultimate tensile strength of CFRP strips has been reached**



In accordance, it was noticed that the strain corresponding to the ultimate bond strength between FRP and concrete substrate, registered experimentally, was lower than the one expected according to the Teng et al. [6] criterion ($8.1\%_{\text{oo}}$).

Regarding the vertical displacement at mid-span, the difference between the analytical and experimental results was around 16.2%. At the first stage of the diagram, the cracking load differ less than 1% while the corresponding displacement at mid-span varied about 2.6%. At the end of the second stage the load difference was close to 3.6% and the displacement at mid-span differ in 9.7%.

Figure [8] and Table [3] show the behavior of beam VFC_PE_01, post-strengthened with two prestressed CFRP strips. In this case, although the analytical and experimental results of the first stage of the diagram have shown a variation of about 47.6%, results for the second and the third stage of the diagram were very close, differing in about 1.4% (for loads) and 2.4% (for the displacement at mid-span) at the end of the second stage and in 1.7% (for loads) and 2.1% (for vertical displacement at mid-span) at the end of the third stage. The post-strengthening of the beam VFC_PE_01 also failed prematurely, due to the *peeling-off* of the prestressed strips. Therefore, the load and the displacement predicted by the analytical procedure were 3.5% and 11% higher than the ones obtained experimentally.

In conclusion, although there are still some differences between analytical and experimental results, especially when peeling-off occurs, it was considered that the analytical data satisfactorily fitted the data obtained experimentally.

5. Conclusions

The data collected in this work points out that the analytical solution developed is suitable to represent the behavior of a post-strengthened beams, although it has resulted in a stiffer behavior for the first stage of the diagram, for beam VFC_PE_01, and in a higher ultimate load for beam VFC_NP_01. Differences of about 16.2% and 11% were observed between the theoretical and the observed values of the vertical displacement at mid-span near failure of beams VFC_NP_01 e VFC_PE_01. Nonetheless, in general, the differences between the estimated and real loads at the cracking, yielding and failure points were lower than 5%.

Considering the natural variability of failure loads, these results clearly indicate that there is a good compatibility between the analytical solution proposed and the experimental results, over the entire range of loads. This conclusion ascertains that the proposed model is useful to simulate the behavior of real post-strengthened beams, with prestressed and non-prestressed strips.

It is interesting to highlight that the failure mode of the post-strengthened beams was fairly well estimated by the model. However, because the model does not consider peeling-off, the ultimate failure load expected was 13.20% and 3.30% higher than the one obtained experimentally, for beams VFC_NP_01 and VFC_PE_01, respectively.

6. Acknowledgements

The authors would like to acknowledge CNPq (Portuguese acronym of the Brazilian Ministry of Science's National Research Coun-

Table 3 – Loads and vertical displacements at mid-span

Beam	Phase of the diagram	P_{exp} (kN)	δ_{exp} (mm)	P_{num} (kN)	δ_{num} (mm)	$\frac{P_{\text{num}}}{P_{\text{exp}}}$	$\frac{\delta_{\text{num}}}{\delta_{\text{exp}}}$
VT	Concret cracking	37,00	3,44	36,97	3,530	0,999	1,026
	Steel yielding	88,00	71,38	89,52	67,540	1,017	0,946
	End of testing*	100,14	219,91	100,14	198,150	1,000	0,901
VFC_NP_01	Concret cracking	37,00	3,44	36,97	3,530	0,999	1,026
	Steel yielding	108,00	76,93	104,21	69,530	0,964	0,903
	Post-Strengthening rupture	127,25	129,48	144,43	150,460	1,132	1,162
VFC_PE_01	Concret cracking	58,00	7,68	57,89	4,031	0,998	0,524
	Steel yielding	128,00	70,87	129,78	69,190	1,014	0,976
	Post-Strengthening rupture	162,41	144,07	167,78	159,950	1,033	1,110

*The simulation of beam VT was finished when the load corresponding to the end of the test was reached.

cil) and CAPES (Portuguese acronym of the Brazilian Ministry of Education's Higher Education Human Resources Development Agency) for providing the financial support needed to develop this project. Authors would also like to express their appreciation for the technical support given by Professor Urs Meier and the research team at EMPA (Swiss Federal Laboratories for Materials Testing and Research), in Switzerland.

7. References

- [01] CHARKAS, H., RASHEEDH, A., MELHEM, H. Simplified Load-deflection calculation of FRP strengthened RC beams based on a rigorous approach. In: 15th ASCE ENGINEERING MECHANICS CONFERENCE, 2002, New York. Anais... New York: 15th ASCE ENGINEERING MECHANICS CONFERENCE, 2002. [CD-Rom]
- [02] CHARKAS, H., RASHEEDH, A., MELHEM, H. Rigorous procedure for calculating deflections of Fiber-Reinforced Polymer-Strengthened reinforced concrete beams. ACI Structural Journal, july/august, 2003. p. 529-539.
- [03] EL-MIHILMY, M. T., TEDESCO, J. W. Deflection of concrete beams strengthened with Fiber-Reinforced Polymer (FRP) plates. ACI Structural Journal, september/october, 2000. p. 679-688.
- [04] RAZAQPUR, A. G., SVECOVÁ, D., CHEUNG, M. S. Rational method for calculating deflection of Fiber-Reinforced Polymer reinforced beams. ACI Structural Journal, january/february, 2000. p. 175-184.
- [05] AMERICAN CONCRETE INSTITUTE. Guide for the Design and Construction of Externally Bonded FRP Systems for Strengthening Concrete Structures: ACI 440.2R-02. Farmington Hills, 2002. 45p.
- [06] TENG, J. G., CHEN, J. F., SMITH, S. T., LAM, L. FRP Strengthened RC Structures. Chichester: Wiley, 2002. 245p.
- [07] GARCEZ, M. R. Alternativas para Melhoria no Desempenho de Estruturas de Concreto Armado Reforçadas pela Colagem de Polímeros Reforçados com Fibras. Porto Alegre: UFRGS, 2007. 241p. Doctorate Thesis (Doctorate in Civil Engineering) – Universidade Federal do Rio Grande do Sul, 2007.